RENORMALIZATION GROUP AND THERMAL FLAVOR PRODUCTION IN QGP*

JOHANN RAFELSKI
Department of Physics, University of Arizona, Tucson, AZ 85721

JEAN LETESSIER and AHMED TOUNSI
Laboratoire de Physique Théorique et Hautes Energies
Université Paris 7, Tour 24, 2 Pl. Jussieu, F-75251 Cedex 05, France

Recent advances in measurements of $\alpha_s(M_Z)$ allow to refine the rates of thermal flavor production in quark-gluon plasma. We employ QCD renormalization group to evaluate the running of QCD parameters $\alpha_s(\mu)$ and $m_i(\mu)$, i = s, c down to and below 1 GeV scale of interest in thermal strangeness production. Using these results we obtain the low density thermal relaxation time for glue based production of s and c quarks and discuss the QGP flavor observable.

1 Introduction

The understanding of (thermal) production of (heavy) flavor and the associated chemical equilibration [1] is of considerable interest as a diagnostic probe of the properties of the deconfined quark-gluon plasma (QGP) phase of strong interactions. QGP formation in relativistic nuclear collisions at sufficiently high energy is expected on basis of (lattice) QCD studies and many other, more phenomenological, explorations of the behavior of strongly interacting particles under extreme conditions.

Our objective here is to obtain a computational framework allowing to eliminate the need for an arbitrary coupling constant in the two particle collision cross section of flavor production [2] and to obtain the relevant two particle rates using running QCD parameters $\alpha_s(\mu)$ and $m_i(\mu)$, i =s, c. While theory and experiment constrain now sufficiently the coupling strength α_s, considerable uncertainty still remains in particular in regard of strange quark mass scale.

The generic angle averaged two particle cross section for (heavy) flavor production processes $g+g \to f+\bar{f}$ and $q+\bar{q} \to f+\bar{f}$, are:

$$\bar{\sigma}_{gg\to f\bar{f}}(s) = \frac{2\pi\alpha_s^2}{3s}\left[\left(1+\frac{4m_f^2}{s}+\frac{m_f^4}{s^2}\right)\tanh^{-1}W(s)-\left(\frac{7}{8}+\frac{31m_f^2}{8s}\right)W(s)\right], \quad (1)$$

$$\bar{\sigma}_{q\bar{q}\to s\bar{s}}(s) = \frac{8\pi\alpha_s^2}{27s}\left(1+\frac{2m_s^2}{s}\right)W(s), \quad (2)$$

*Presented at 3rd American University Paris Workshop on QCD 3-8 Jun 1996. Paris, France; In press pp.388-397 in *QCD: Collisions, confinement and chaos* Edited by H.M. Fried and B. Muller (World Scientific, 1997)

where $W(s) = \sqrt{1 - 4m_{\rm f}^2/s}$, and both the QCD coupling constant $\alpha_{\rm s}$ and flavor quark mass $m_{\rm f}$ will be in this work the running QCD parameters. In this way a large number of even-$\alpha_{\rm s}$ diagrams contributing to flavor production is accounted for.

What remains unaccounted in our work is another class of processes in which at least one additional gluon is present. While only in very high density environment we could imagine relevant contributions from three body initial state collisions, presence of an additional soft gluon in the final state remains unaccounted for today. Leading diagrams contain odd powers of $\alpha_{\rm s}$ and their generic cross section is in general infrared divergent, requiring a cut-off which for processes occurring in matter is provided by the interactions (dressing) with other particles present. The process in which a massive 'gluon', that is a quasi-particle with quantum numbers of a gluon, decays into a strange quark pair, is partially included in the resummation that we accomplish in the present work. At the present time we do not see a systematic way to incorporate any residue of this and other effects, originating in matter surrounding the microscopic processes, as work leading to understanding of renormalization group equations in matter (that is at finite temperature and/or chemical potential) is still in progress.[3]

We discuss in next section the running of mass and coupling constant and turn to the evaluation and discussion of the relaxation times for flavor production in section 3. We discuss the relevance of the flavor observable of QGP and describe how these relaxation times allow to compute the hadronic particle yields in section 4.

2 Running QCD Parameters

To determine the two QCD parameters required, we will use the renormalization group functions β and $\gamma_{\rm m}$:

$$\mu\frac{\partial\alpha_{\rm s}}{\partial\mu} = \beta(\alpha_{\rm s}(\mu))\,, \qquad \mu\frac{\partial m}{\partial\mu} = -m\,\gamma_{\rm m}(\alpha_{\rm s}(\mu))\,. \tag{3}$$

For our present study we will use the perturbative power expansion in $\alpha_{\rm s}$:

$$\beta^{\rm pert} - \alpha_{\rm s}^2\,[\,b_0 + b_1\alpha_{\rm s} + \ldots\,]\,, \quad \gamma_{\rm m}^{\rm pert} = \alpha_{\rm s}\,[\,c_0 + c_1\alpha_{\rm s} + \ldots\,]\,, \tag{4}$$

For the SU(3)-gauge theory with $n_{\rm f}$ fermions the first two terms (two 'loop' order) are renormalization scheme independent and we will restrict our study to this order in this report:[4,5]

$$b_0 = \frac{1}{2\pi}\left(11 - \frac{2}{3}n_{\rm f}\right)\,, \quad b_1 = \frac{1}{4\pi^2}\left(51 - \frac{19}{3}n_{\rm f}\right)\,, \tag{5}$$

$$c_0 = \frac{2}{\pi}\,, \qquad c_1 = \frac{1}{12\pi^2}\left(101 - \frac{10}{3}n_{\rm f}\right)\,. \tag{6}$$

The number $n_{\rm f}$ of fermions that can be excited, depends on the energy scale μ. We have implemented this using the exact phase space form appropriate for the terms linear in $n_{\rm f}$:

$$n_{\rm f}(\mu) = 2 + \sum_{i=s,c,b,t} \sqrt{1-\frac{4m_i^2}{\mu^2}}\left(1+\frac{2m_i^2}{\mu}\right)\Theta(\mu-2m_i)\,, \tag{7}$$

with $m_{\rm s} = 0.16\,{\rm GeV}$, $m_{\rm c} = 1.5\,{\rm GeV}$, $m_b = 4.8\,{\rm GeV}$. We checked that there is very minimal impact of the running of the masses in Eq. (7) on the final result, and will therefore not introduce that 'feed-back' effect into our current discussion. The largest effect on our solutions comes from the bottom mass, since any error made at about 5 GeV is amplified most. However, we find that this results in a scarcely visible change even when the mass is changed by 10% and thus one can conclude that the exact values of the masses and the nature of flavor threshold is at present of minor importance in our study.

We show the result of numerical integration for $\alpha_{\rm s}$ in the top portion of Fig. 1. First equation in (3) is numerically integrated beginning with an initial value of $\alpha_{\rm s}(M_Z)$. We use in this report the August 1996 World average:[6] $\alpha_{\rm s}(M_Z) = 0.118$ for which the estimated error is ± 0.003. This value is sufficiently precise to eliminate much of the uncertainty that has befallen much of our earlier studies.[2,7] In addition, the thin solid lines present results for $\alpha_{\rm s}(M_Z) = 0.115$ till recently the preferred result in some analysis, especially those at lower energy scale. As seen in Fig. 1, the variation of $\alpha_{\rm s}$ with the energy scale is substantial, and in particular we note the rapid change at and below $\mu = 1$ GeV, where the strange quark flavor formation occurs in hot QGP phase formed in present day experiments at 160–200 A GeV (SPS-CERN). Clearly, use of constant value of $\alpha_{\rm s}$ is hardly justified, and the first order approximation often used:

$$\alpha_{\rm s}(\mu) \equiv \frac{2b_0^{-1}(n_{\rm f})}{\ln(\mu/\Lambda_0(\mu))^2}\,, \tag{8}$$

leads to a strongly scale dependent $\Lambda_0(\mu)$ shown in the middle section of Fig. 1. Thus it also cannot be used in the evaluation of thermal strangeness and charm production.

With $\alpha_{\rm s}(\mu)$ from the solutions described above, we integrate the running of the quark masses, the second equation in (3). Because the running mass equation is linear in m, it is possible to determine the universal quark mass scale factor

$$m_{\rm r} = m(\mu)/m(\mu_0)\,. \tag{9}$$

Since $\alpha_{\rm s}$ refers to the scale of $\mu_0 = M_Z$, it is a convenient reference point also for quark masses. As seen in the bottom portion of Fig. 1, the change in the quark mass factor is highly relevant, since it is driven by the rapidly changing $\alpha_{\rm s}$ near to $\mu \simeq 1$ GeV. For each of the different functional dependences $\alpha_{\rm s}(\mu)$ we obtain a different function $m_{\rm r}$. The significance of the running of the charmed quark mass cannot be stressed enough, especially for thermal charm production occurring in foreseeable future experiments well below threshold, which amplifies the importance of exact value of $m_{\rm c}$.

Given these results, we find that for $\alpha_{\rm s} = 0.118$ and $m_{\rm s}(M_Z) = 90 \pm 18$ MeV a low energy strange quark mass $m_{\rm s}(1\,{\rm GeV}) \simeq 200 \pm 40$ MeV, in the middle of the standard

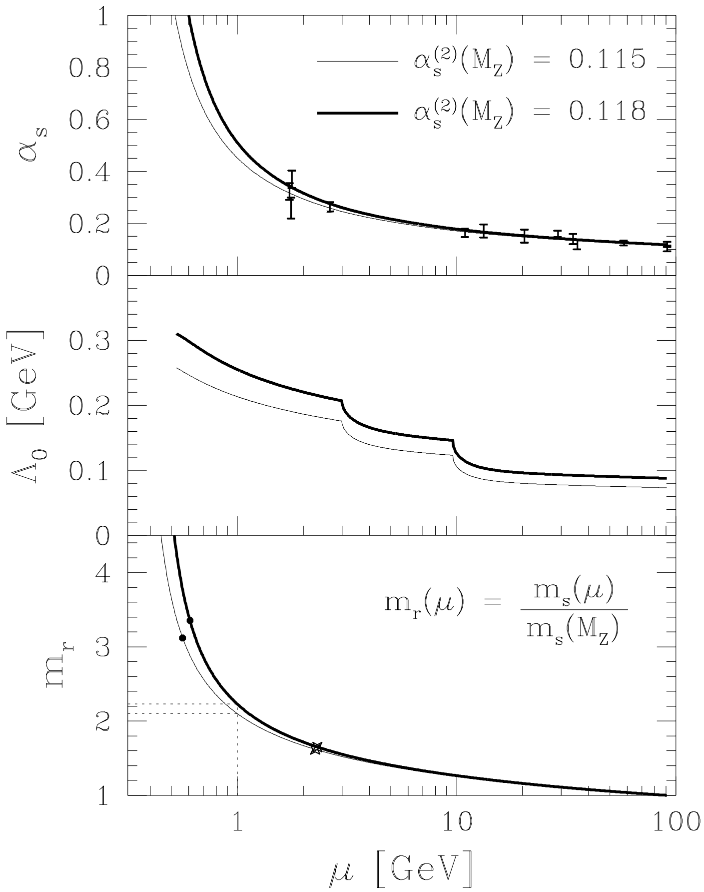

Figure 1: $\alpha_s(\mu)$ (top section); the equivalent parameter Λ_0 (middle section) and $m_r(\mu) = m(\mu)/m(M_Z)$ (bottom section) as function of energy scale μ. Initial value $\alpha_s(M_Z) = 0.118$ (thick solid lines) and $\alpha_s(M_Z) = 0.115$ (thin solid lines). In lower section the dots indicate the strangeness pair production thresholds for $m_s(M_Z) = 90$ MeV, while crosses indicate charm pair production thresholds for $m_c(M_Z) = 700$ MeV.

range $100 < m_s(1\,\text{GeV}) < 300$ MeV. Similarly we consider $m_c(M_Z) = 700 \pm 50$ MeV, for which value we find the low energy mass $m_c(1\,\text{GeV}) \simeq 1550 \pm 110$ MeV, at the upper (conservative for particle production yield) end of the standard range $1 < m_c(1\,\text{GeV}) < 1.6$ MeV. There is another nonperturbative impact of mass running, related to the mass at threshold for pair production m_i^{th}, $i =$ s, c, arising from the solution of:

$$m_i^{\text{th}}/m_i(M_Z) = m_r(2m_i^{\text{th}})\,. \tag{10}$$

This effect stabilizes strangeness production cross section in the infrared: below $\sqrt{\text{s}} = 1$ GeV the strange quark mass increases rapidly and the threshold mass is considerably greater than $m_s(1$ GeV). We obtain the threshold values $2m_s^{\text{th}} = 605$ MeV for $\alpha_s(M_Z) = 0.118$ and $2m_s^{\text{th}} = 560$ MeV for $\alpha_s(M_Z) = 0.115$. Both values are indicated by the black dots in Fig. 1. For charm, the running mass effect plays

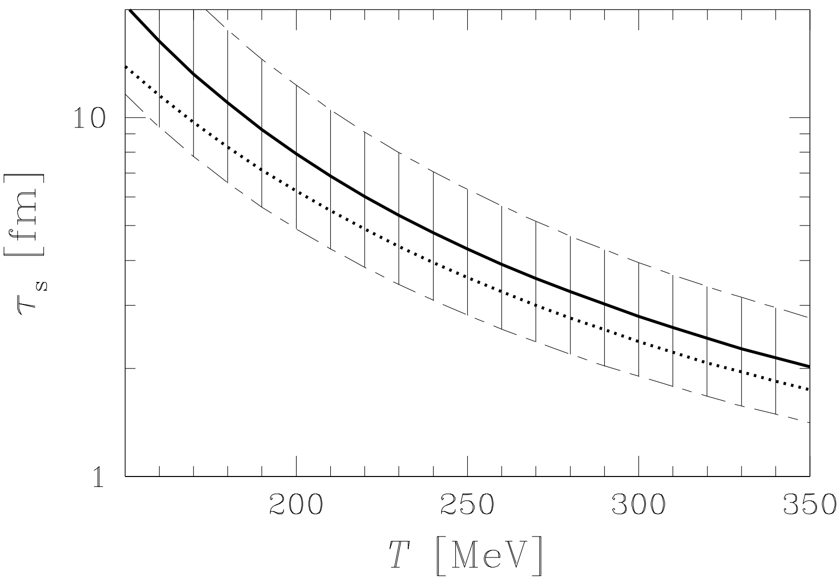

Figure 2: QGP strangeness relaxation time, for $\alpha_s(M_Z) = 0.118$, (thick line) and $=$ 0.115 (thin line); $m_s(M_Z) = 90$ MeV. Hatched areas: effect of variation of strange quark mass by 20%. Dotted: comparison results for fixed $\alpha_s = 0.5$ and $m_s = 200$ MeV.

differently: since the mass of charmed quarks is listed in tables for $\mu = 1$ GeV, but the value of the mass is above 1 GeV, the production threshold mass is smaller than expected (i.e., listed value). For $m_c(M_Z) = 700$ MeV the production threshold is found at $\sim 2m_c^{\rm th} \simeq 2.3$ GeV rather than 3.1 GeV that would have been expected for the $m_c(1\ \mathrm{GeV})$. This reduction in threshold enhances thermal production of charm, especially so at low temperatures.

3 Strangeness and Charm Thermal Relaxation Times

The thermal average of the cross section is the invariant production rate per unit time and volume:

$$\begin{aligned} A_s &\equiv A_{gg} + A_{u\bar{u}} + A_{d\bar{d}} + \ldots \\ &= \int_{4m_s^2}^{\infty} ds 2s\delta(s-(p_1+p_2)^2) \int \frac{d^3p_1}{2(2\pi)^3E_1} \int \frac{d^3p_2}{2(2\pi)^3E_2} \\ &\qquad \times \left[\frac{1}{2}g_g^2 f_g(p_1)f_g(p_2)\overline{\sigma_{gg}}(s) + n_f g_q^2 f_q(p_1) f_{\bar{q}}(p_2)\overline{\sigma_{q\bar{q}}}(s) + \ldots\right] . \qquad (11) \end{aligned}$$

The dots indicate that other mechanisms may contribute to strangeness production. The particle distributions f_i are in our case thermal Bose/Fermi functions (for fermions with $\lambda_q = 1.5$), and $g_q = 6$, $g_g = 16$. For strangeness production $n_f = 2$, and for charm production $n_{\rm f} = 3$. From the invariant rate we obtain the strangeness relaxation time $\tau_{\rm s}$ shown in Fig. 2, as function of temperature:

$$\tau_{\rm s} \equiv \frac{1}{2} \frac{\rho_{\rm s}^{\infty}(\tilde{m}_{\rm s})}{(A_{gg} + A_{qq} + \ldots)}\,. \tag{12}$$

Note that here unaccounted for processes, such as the above mentioned odd-order in $\alpha_{\rm s}$ would add to the production rate incoherently, since they can be distinguished by the presence of incoming/outgoing gluons. Thus the current calculation offers an upper limit on the actual relaxation time, which may still be smaller. In any case, the present result suffices to confirm that strangeness will be very near to chemical equilibrium in QGP formed in collisions of large nuclei.

We show in Fig. 2 also the impact of a 20% uncertainty in $m_{\rm s}(M_Z)$, indicated by the hatched areas. This uncertainty is today much larger compared to the uncertainty that arises from the recently improved precision of the strong coupling constant determination.[6] We note that the calculations made[1] at fixed values $\alpha_{\rm s} = 0.5$ and $m_{\rm s} = 200$ MeV (dotted line in Fig. 2) are well within the band of values related to the uncertainty in the strange quark mass.

Since charm is somewhat more massive compared to strangeness, there is still less uncertainty arising in the extrapolation of the coupling constant. Also the systematic uncertainty related to the soft gluons (odd-$\alpha_{\rm s}$) terms are smaller, and thus the relaxation times $\tau_{\rm c}$ we show in Fig. 3 are considerably better defined compared to $\tau_{\rm s}$. There is also less relative uncertainty in the value of charm mass. We also show in Fig. 3 (dotted lines) the fixed $m_{\rm c}$, $\alpha_{\rm s}$ results with parameters selected to border high and low T limits of the results presented. It is difficult to find a good comparative behavior of $\tau_{\rm c}$ using just one set of $m_{\rm c}$ and $\alpha_{\rm s}$. This may be attributed to the importance of the mass of the charmed quarks, considering that the threshold for charm production is well above the average thermal collision energy, which results in emphasis of the effect of running charm mass. In the high T-limit the choice (upper doted line in Fig. 3) $m_{\rm c} = 1.5$ GeV, $\alpha_{\rm s} = 0.4$ is appropriate, while to follow the result at small T (lower doted line in Fig. 2) we take a much smaller mass $m_{\rm c} = 1.1$ GeV, $\alpha_{\rm s} = 0.35$.

We recall that the equilibrium distribution is result of Boltzmann equation description of two body collisions. Thus the mass arising in the equilibrium density $\rho_{\rm s}^{\infty}$ in Eq. (12) is to be taken at the energy scale of the average two parton collision. We adopt for this purpose a fixed value $\tilde{m}_{\rm s} = 200$ MeV, and observe that in the range of temperatures here considered the precise value of the mass is insignificant, since the quark density is primarily governed by the T^3 term in this limit, with finite mass correction being $\mathcal{O}(10\%)$. The situation is less clear for charm relaxation, since the running of the mass should have a significant impact. Short of more complete kinetic treatment, we used $m_{\rm c} \simeq 1.5$ GeV in order to establish the reference density $\rho_{\rm c}^{\infty}$ in Eq. (12).

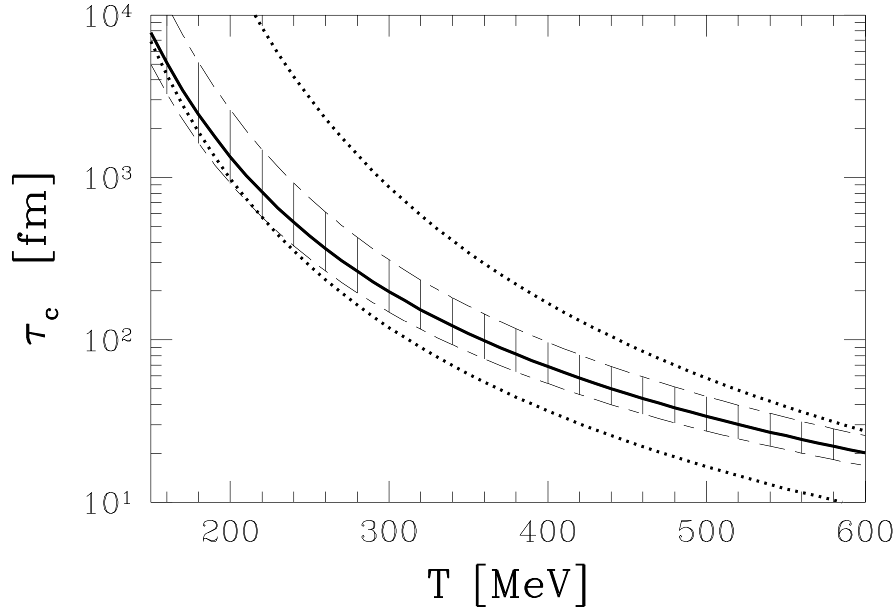

Figure 3: Solid lines: thermal charm relaxation constant in QGP, calculated for running $\alpha_s(M_Z) = 0.115$; 0.118, (indistinguishable), $m_{\rm c}(M_Z) = 700$ MeV. Lower dotted line: for fixed $m_{\rm c} = 1.1$ GeV, $\alpha_{\rm s} = 0.35$; upper doted line: for fixed $m_{\rm c} = 1.5$ GeV, $\alpha_{\rm s} = 0.4$. Hatched area: effect of variation $m_{\rm c}(M_Z) = 700 \pm 50$ MeV

4 QGP Flavor Observable

We will indicate in this section how the study of flavor production impacts our understanding and diagnosis of the deconfined QGP phase. We recall first that there are two generic flavor observable which we can study analyzing experimental data:

- yield of strangeness/charm:
  once produced in hot early QGP phase, strangeness/charm is not reannihilated in the evolution of the deconfined state towards freeze-out, and thus the flavor yield is characteristic of the initial, most extreme conditions;
- phase space occupancy $\gamma_{\rm s,c}$:
  impacts distribution of flavor among final state particle abundances.

Given that the thermal equilibrium is established within a considerably shorter time scale than the (absolute) heavy flavor chemical equilibration, we can characterize the equilibration of the phase space occupancy by an average over the momentum distribution:

$$\gamma_i(t) \equiv \frac{\int d^3p\, d^3x\, n_i(\vec{p}, \vec{x}; t)}{\int d^3p\, d^3x\, n_i^\infty(\vec{p}, \vec{x})}\,, \quad i = {\rm s},\, {\rm c}\,. \tag{13}$$

The chemical equilibrium density is indicated by upper-script '∞'. When several carriers of the flavor are present, as is the case in the confined phase, n_i is understood to comprise a weighted sum.

In order to be able to compute the production and evolution of strangeness and charm flavor a more specific picture of the temporal evolution of dense matter is needed. Here, we will address specifically strangeness production in collisions at CERN-SPS, up to 200 A GeV per nucleon. We use a simple, qualitative description, simplified by the assumption that the properties of the hot, dense matter are constant across the entire volume (fireball model). We consider radial expansion to be the dominant factor for the evolution of the fireball properties such as temperature/energy density and lifetime of the QGP phase. The expansion dynamics follows from two assumptions:

- the (radial) expansion is entropy conserving, thus the volume and temperature satisfy:
$$V \cdot T^3 = \text{ Const.} \tag{14}$$
- the surface flow velocity is given by the sound velocity in a relativistic gas
$$v_{\mathrm{f}} = 1/\sqrt{3}\,. \tag{15}$$

This leads to the explicit forms for the radius of the fireball and its average temperature:

$$R = R_{\mathrm{in}} + \frac{1}{\sqrt{3}}(t - t_{\mathrm{in}})\,, \qquad T = \frac{T_{\mathrm{in}}}{1 + (t - t_{\mathrm{in}})/\sqrt{3}R_{\mathrm{in}}}\,. \tag{16}$$

The initial conditions:

$$\begin{aligned} T_{\mathrm{in}} &= 320 \ \ \mathrm{MeV};\ \ R_{\mathrm{in}} = 5.6\,\mathrm{fm};\ \ t_{\mathrm{in}} = 1\,\mathrm{fm}/c;\ \ \lambda_{\mathrm{q}} = 1.6;\ \text{ for Pb–Pb}\,, \\ T_{\mathrm{in}} &= 280 \ \ \mathrm{MeV};\ \ R_{\mathrm{in}} = 4.7\,\mathrm{fm};\ \ t_{\mathrm{in}} = 1\,\mathrm{fm}/c;\ \ \lambda_{\mathrm{q}} = 1.5;\ \text{ for S–Pb/W}\,, \end{aligned}$$

are derived from our exploration [8] of the equations of state of QGP: the radius R_{in} has been determined such that the baryon number content in the fireball is 380 (Pb–Pb case) and 120 (S–Pb/W case) respectively, corresponding to ‘zero’ impact parameter collisions.

In the fireball in every volume element we have:

$$n_{\mathrm{s}}(\vec{p};t) = \gamma_{\mathrm{s}} n_{\mathrm{s}}^{\infty}(\vec{p};T,\mu_{\mathrm{s}})\,. \tag{17}$$

In this limit and allowing for the detailed balance reactions, thus re-annihilation of flavor, the yield is obtained from the equation:

$$\frac{dN_{\mathrm{s}}(t)}{dt} = V(t) A_{\mathrm{s}} \left[1 - \gamma_{\mathrm{s}}^2(t)\right]\,. \tag{18}$$

Allowing for dilution of the phase space density in expansion, we derive [7] from Eq. (18) an equations describing the change in $\gamma_{\mathrm{s}}(t)$:

$$\frac{d\gamma_{\mathrm{s}}}{dt} = \left(\gamma_{\mathrm{s}} \frac{\dot{T} m_{\mathrm{s}}}{T^2} \frac{d}{dx} \ln x^2 K_2(x) + \frac{1}{2\tau_{\mathrm{s}}}\left[1 - \gamma_{\mathrm{s}}^2\right]\right)\,. \tag{19}$$

Here K_2 is a Bessel function and $x = m_\mathrm{s}/T$. Note that even when $1-\gamma_\mathrm{s}^2 < 1$ we still can have a positive derivative of γ_s, since the first term on the right hand side of Eq. (19) is always positive, both $\dot{T}$ and $d/dx(x^2 k_2)$ being always negative. This shows that dilution due to expansion effects in principle can make the value of γ_s rise above unity.

Given the relaxation constant $\tau_\mathrm{s}(T(t))$, these equations can be integrated numerically. We found [7] in analysis of S-W collisions at 200A GeV $\gamma_\mathrm{s}^\mathrm{exp} \simeq 0.75$, and moreover, for S–Ag collisions at 200A GeV a recent evaluation of the specific strangeness yield leads to $N_\mathrm{s}/B|^\mathrm{exp} = 0.86 \pm 0.14$ (see table 4 of Ref. [10]). Both results are well reproduced within our simple dynamical model.[7]

Assuming that the model we proposed is thus tested at 200 A GeV, we compute the strangeness yield and phase space occupancy as function of energy. This allows to evaluate the strange (anti)baryon yields from QGP as function of collision energy. We note that at fixed $m_\perp$ the medium dependent factor controlling the abundance of hadrons emerging from the surface of the deconfined region is related to the chemical conditions in the source, and for strange quarks, there is also the occupancy factor γ_s to be considered:

$$n_h|_{m_\perp} = e^{-m_\perp/T} \prod_{k\in h} \gamma_k \lambda_k \,. \tag{20}$$

The strange quark fugacity is in deconfined phase unity, while the light quark fugacity evolution with energy of colliding ions follows from our earlier studies.[8] In Fig. 4. we have normalized all yields at $E_\mathrm{Lab} = 158$A GeV. Remarkably, all antibaryon yields (left hand side of Fig. 4) cluster together (solid lines: (anti)nucleons, long dashed: (anti)hyperons, short-dashed: (anti)cascades, and dotted: (anti)omegas), thus as long as the QGP phase is formed, ratios of rare multi strange antibaryons should not change significantly while the collision energy is reduced, until the QGP formation is disrupted. It should be noted that the yield of $\overline{\Omega}$ remains appreciable, all the way even at very small energies — this is the case as long as these particles are produced by the deconfined phase, rather than in individual hadronic interactions. For baryons (right hand side of Fig. 4) there is considerable differentiation of the yield behavior: the reference yield of nucleons remains constant, as it is intuitively expected, but the yield of more strange baryons decreases with energy.

5 Final Remarks

Using QCD renormalization group methods we have studied the flavor (s, c) chemical equilibrium relaxation times. We have shown that the newly measured QCD coupling constant comprises sufficiently small uncertainty to allow precise evaluation of strangeness production at and below 1 GeV energy scale. Our study has further proven that it is essential to incorporate in the evaluation of flavor production rates both running mass *and* running coupling constant.

We find that running of the QCD parameters is of major significance, since, e.g., the effective charm production mass is considerably reduced, seen on the scale of

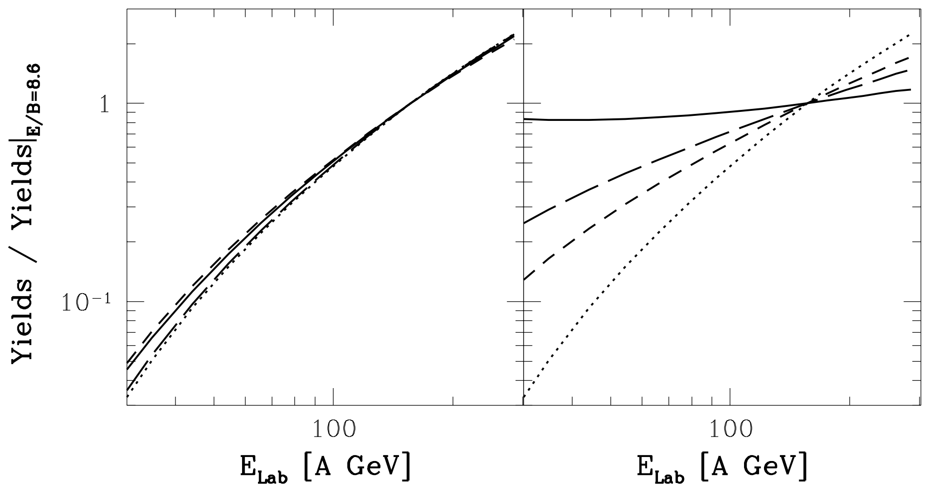

Figure 4: Relative yields of antibaryons (left) and baryons (right) as function of heavy ion collision energy $E_{\rm Lab}$. Abundance set to a common value (unity) at $E_{\rm Lab} = 158$A GeV. Solid lines nucleons, long dashed $\Lambda+\Sigma^0$, short dashed Ξ, dotted Ω.

available thermal energies. We found considerable enhancement of charm production for temperatures applicable at SPS collision energy, compared to fixed mass results. While charm experiences at low temperature $T \simeq 200$ MeV a 100 times slower approach to chemical equilibrium compared to strangeness, for temperatures of about 500 MeV, as may apply to the conditions generated at LHC or perhaps even RHIC colliders, $\tau_{\rm c} \to 30$ fm, which is within factor two of the expected maximum lifespan of the deconfined state. Thus our calculations suggest that there will be a significant abundance of thermal charm in nuclear interactions at RHIC/LHC. In consequence, open charm should play a similar role in the diagnosis of the 'hot' $T \simeq 500$ MeV deconfined state as strangeness is playing today for the 'cold' $T \simeq 250$ MeV case, and charm equilibrium appears within reach of the extreme conditions possibly arising at LHC.

Our here presented and other results [7] imply that in key features the strange particle production results obtained at 160–200A GeV, are consistent with the QGP formation hypothesis. However, in order to ascertain the possibility that indeed the QGP phase is already formed today, a more systematic experimental exploration as function of collision energy of the different observable is required, for which purpose we also have explored the collision energy dependence of the most characteristic strange particle features expected from the QGP phase.

Acknowledgments

J.R. acknowledges partial support by DOE, grant DE-FG03-95ER40937.
LPTHE: Unité associée au CNRS UA 280.

References

[1] T. Biró and J. Zimányi, *Phys. Lett.* **B113** (1982) 6; *Nucl. Phys.* **A395** (1983) 525;
J. Rafelski and B. Müller, *Phys. Rev. Lett.* **48** (1982) 1066; **56** (1986) 2334E.

[2] J. Letessier, J. Rafelski, and A. Tounsi, *Impact of QCD and QGP properties on strangeness production,* Phys. Lett. B. *in press* (1996).

[3] P. Elmfors and R. Kobes, Phys. Rev. **D51**, 774 (1995).

[4] I. Hinchliffe, Quantum Chromodynamics, in: L. Montanet *et al.*, Phys. Rev. **D50** (1994) 1173 (update August 1995: http://pdg.lbl.gov/); see also, e.g., T. Muta, *Foundations of Quantum Chromodynamics*, (World Scientific 1987).

[5] L.R. Surguladze and M.A. Samuel, Rev. Mod. Phys. **68** (1996) 259.

[6] M. Schmelling, *Status of the Strong Coupling Constant*, presented at 28th International Conference on High Energy Physics, Warsaw, July 1996, to appear in proceedings, A.K. Wróblewski et al., eds.

[7] J. Rafelski, J. Letessier and A. Tounsi, *Acta Phys. Pol.* **B27** (1996) 1035; and references therein.

[8] J. Letessier, J. Rafelski, and A. Tounsi, *Phys. Lett.* **B333**, 484 (1994); **B323**, 393 (1994).

[9] J. Rafelski, *Phys. Lett.* **B262** (1991) 333; *Nucl. Phys.* **A544** (1992) 279c.

[10] M. Gaździcki and D. Röhrich, *Strangeness in Nuclear Collisions* preprint IKF-HENPG/8-95, *Z. Physik* C (1996).